Physics of Plasmas ACCEPTED MANUSCRIPT
This is the author's peer reviewed, accepted manuscript. However, the online version of record will be different from this version once it has been copyedited and typeset.
PLEASE CITE THIS ARTICLE AS DOI: 10.1063/5.0104879
AIP Publishing

On the impact of electric field fluctuations on microtearing turbulence

M. Hamed,[1] M.J. Pueschel,[1, 2] J. Citrin,[1] M. Muraglia,[3] X. Garbet,[4] and Y. Camenen[3]
[1]*Dutch Institute for Fundamental Energy Research, 5612 AJ Eindhoven, The Netherlands*
[2]*Science and Technology of Nuclear Fusion Group, Eindhoven University of Technology, 5612 AP Eindhoven, The Netherlands*
[3]*Aix-Marseille University, CNRS, PIIM UMR 7345, Marseille, France*
[4]*CEA, IRFM, F-13108 St-Paul-Lez-Durance, France*

The magnetic drift and the electric potential play an important role in microtearing destabilization by increasing the growth rate of this instability in the presence of collisions, while in electrostatic plasma micro-turbulence, zonal electric potentials can have a strong impact on turbulent saturation. A reduced model has been developed showing that the Rechester-Rosenbluth model is a good model for the prediction of electron heat diffusivity by microtearing turbulence. Here, nonlinear gyrokinetic flux-tube simulations are performed in order to compute the characteristics of microtearing turbulence and the associated heat fluxes in tokamak plasmas and to assess how zonal flows and zonal fields affect saturation. This is consistent with a change in saturation mechanism from temperature corrugations to zonal-fields and zonal-flows based energy transfer. It is found that removing the electrostatic potential causes a flux increase, while linearly stabilization is observed.

m.hamed@differ.nl

I. INTRODUCTION

In magnetic confinement fusion research, the causes of electron heat transport are still not fully understood. In H-mode[1,2] tokamak plasmas, electron fluxes can be driven by a variety of instabilities covering a large range of temporal and spatial scales. In H-mode, accurate modeling of pedestal dynamics is essential in predicting temperature and density profiles. Several studies on the origin of the electron heat transport in the pedestal region[3–6,8–14] show that drift-wave instabilities, such as the electron-temperature-gradient (ETG) instability, the trapped-electron mode (TEM) and the kinetic-ballooning mode (KBM), can explain the electron heat transport observed experimentally. These instabilities can develop in the pedestal region, leading to turbulence, which affects the transport and the confinement of heat and particles.

Presently, models based on the stability of large-scale magnetohydrodynamic modes are commonly used to describe the pedestal region[15,16]. Due to the various possible instabilities and disparity of scales, the full pedestal characterization (in terms of its width and height) is still an open issue. In particular, small-scale instabilities, such as the microtearing (MT) mode, need to be taken into account. MTs are small-scale tearing type instabilities driven by the electron temperature gradient with toroidal mode numbers larger than conventional tearing modes. MT modifies the magnetic-field-line topology at the ion-Larmor-radius scale and leads to the formation of magnetic islands. The discovery of collisional MT driven by the electron temperature gradient is attributed to Hazeltine et al.[17] in 1975. They proposed a kinetic description of a slab current sheet destabilized by an electron temperature gradient leading to instability in the collisional regime only, triggering several subsequent developments of linear MT stability theory[18–27]. Recently, the linear theory of slab MT modes using a kinetic approach has been successfully compared with linear gyrokinetic simulations[28]. The linear stability of the collisionless MT predicted by the theory was found to be consistent with numerical simulations[29] using the gyrokinetic code GKW[30]. Starting with this simple model, the magnetic drift and the electric potential were included progressively in the analytical calculation. Without the electric potential, the magnetic drift was found to be destabilising, but only in conjunction with finite collisionality. Then, with both electric potential and magnetic drift, the current inside the resistive layer was evaluated from a system of two equations linking the magnetic vector potential (and, as a the consequence, the current) and the electric potential. This system of equations was then solved numerically using an eigenvalue code. Good agreement between the analytical calculation and GKW simulations was found. This indicates that the magnetic drift velocity and electric potential fluctuations are destabilizing when combined with collisions[31].

In gyrokinetic simulations, MT were found unstable in the conventional tokamaks JET[7,8,11], ASDEX Upgrade[32,33], and DIII-D[34–37], in spherical tokamaks[38–48], and in the reversed-field pinch[49,50]. Recently, different techniques have been developed to track magnetic fluctuations in JET[7] or the dynamical frequency evolution of MT in DIII-D[36], in order to validate nonlinear simulations against tokamak pedestal data and leading to a quantitative description of the experimentally observed magnetic fluctuations, highlighting the need to determine the role played by this micro-instability in transport and confinement.

The evaluation and calculation of heat fluxes in the pedestal using nonlinear gyrokinetic codes is computationally expensive. To obtain nonlinear fluxes at a single radius, the computational cost is around 10^5 CPUh. Reduced models are essential to enable broad and transport-time-scale studies and need to capture essential linear and nonlinear properties of the system. Such reduced models are commonly based on the quasilinear (QL) approximation, assuming that the phase difference between fluctuating fields (e.g, n and ϕ for the E $\times$ B particle flux) is similar

PLEASE CITE THIS ARTICLE AS DOI: 10.1063/5.0104879

in the linear and nonlinear regimes for the wavenumbers that drive the majority of the transport. Presently, quasilinear transport models are focused on electrostatic micro-instabilities providing good agreement with both experimental results by reproducing experimental profiles and nonlinear gyrokinetic simulations[52,53]. A QL transport model accounting for the electrostatic fluxes produced by KBM has been developed, however for MT the development of QL models is challenging, and presently, in the pedestal no standard model exists. However, several QL transport models have been developed and tested against nonlinear simulations of MT turbulence, including one based on a fluid approach, with slab geometry and strong collisionality[54], as well as one in an idealized tokamak core plasma scenario[55].

These results lay the foundation for efficient computation of MT fluxes. The next, important step is to expand on this ad-hoc approach by providing model refinement and a more solid theoretical foundation. For that, we proposed to relate the fluxes to the linear functional that was used for studying the linear stability of microtearing[31]. These results will enable more reliable fast predictions as to the turbulent fluxes produced in MT turbulence. Zonal flows (ZFs) are $n = 0$, $m = 0$ (referring to the toroidal and poloidal mode number, respectively) electric field fluctuations[56] (ZFs) and cannot tap the free energy stored in temperature or density gradients; instead, ZFs are driven exclusively by nonlinear interactions[57]. The generation of ZFs acts to reduce the intensity and level of turbulent transport by regulating drift-wave turbulence. Zonal flows are sheared flows generated by turbulence and appear as a radial variation of the electric potential, but with no toroidal variation (constant on the magnetic flux surface). Indeed, in tokamak plasmas, the turbulence driven by ion-temperature-gradient modes (ITGs) and TEMs can be regulated or suppressed by zonal flows[58], thus allowing an improvement of the plasma confinement. More precisely, the zonal mode catalyzes energy transfer to modes at higher radial wavenumber but still at the large scales of instability, with stable eigenmodes absorbing significant energy (see, e.g., Refs.[4,59–61]). In addition to the zonal flow, the turbulence can also generate, by a similar mechanism, zonal magnetic fields. Like the zonal flow, the zonal field fluctuates homogeneously on the flux surface. Zonal fields can react back on the turbulence via a process of corrugated magnetic shearing[62,63]. For ITG and TEM turbulence, zonal fields tend to have limited impact[62,64,65].

In this context, it should be noted that, numerically, the modeling of MTs can be challenging. The small width of the current layer and the sensitivity of magnetic reconnection to dissipation imply the need for high numerical resolution and weak numerical dissipation[66], especially at low collisionality.

The purpose of this work is to evaluate transport due to MT turbulence in tokamaks and the impact of zonal-flow and zonal-field dynamics. The remainder of this paper is structured as follows. In Section II, the linear stability of MT modes is evaluated using a variational form of the Vlasov equation and Ampère's law. Then, in order to model fluxes due to MT turbulence, a quasilinear transport model is developed which relates fluxes to a functional that can be used for studying the linear stability of MT. Section III compares the analytical predictions with nonlinear simulations of core MT turbulence. The objective is to understand how the magnetic fluctuation level is linked to the associated electron heat transport. In Section IV, the effect of the electric potential in nonlinear saturation is investigated. The electron heat flux increases when the electric potential is switched off, whereas the converse would be expected on the basis of linear stability analysis. This suggests that electric potential fluctuations can play a role in the nonlinear regulation of microtearing turbulence. Similarly, the effect of zonal magnetic fields is discussed.

II. QUASILINEAR MODEL OF MICROTEARING MODES

A. Linear stability of microtearing modes

Both the magnetic drift and the electric potential play an important role in MT physics by increasing the growth rate of this microinstability in the presence of collisions. To quantify these properties, a linear model is used based on the calculations in Ref.[31]. A simple geometry of circular concentric flux surfaces is used, where r is the minor radius of the flux surface of interest, φ the toroidal angle, and θ the straight-field-line poloidal angle. Any perturbed field, for instance the vector potential $A_\parallel$, at a given toroidal wave number n and complex frequency ω can be written as

$$A_\parallel(r,\alpha,\theta,t) = \sum_{p=-\infty}^{\infty} \hat{A}_\parallel(\theta+2p\pi)\mathrm{e}^{in(\varphi-q(\theta-\theta_k+2p\pi))-i\omega t} \tag{1}$$

Here, $\alpha = \varphi - q(r)\theta$ is a transverse coordinate, θ plays the role of a coordinate along the unperturbed field lines, q is the safety factor near the rational surface $q = m/n$, and θ_k is the ballooning angle[21]. The perturbed current along the magnetic field line $J_\parallel = \sum_i e_i \int d^3v f_i v_\parallel$ is obtained from the distribution function of each charged species i, whose evolution is given by the Fokker-Planck equation. The distribution function f for each species at a given n and ω is split into an unperturbed part F_M, taken as an unshifted Maxwellian of temperature T_{eq}, and a perturbed part $\hat{f}_{n\omega(\theta,v_\parallel,\mu)}$, where $v_\parallel$ is the parallel velocity and μ the magnetic moment. The perturbed distribution function $\hat{f}_{n\omega}$ is itself written as the sum of an adiabatic part and a resonant part, $\hat{f}_{n\omega} = \mathrm{f}_\mathrm{ad} + \bar{\mathrm{g}}_{\mathrm{n}\omega}$. $\hat{A}_\parallel$ and $\hat{\phi}$, respectively, determine the perturbed magnetic and electric fields: $\hat{\mathbf{B}} = \nabla \times (\hat{A}_\parallel \mathbf{b})$ and $\hat{\mathbf{E}} = -\nabla\hat{\phi} - \partial\hat{A}_\parallel/\partial t$. The resonant part $\bar{g}_{n\omega}$, is the solution of the kinetic equation

$$\left(\omega - k_\parallel v_\parallel - \omega_\mathrm{d}\right)\bar{g}_{n\omega} = \frac{F_M}{T_{eq}}\left(\omega-\omega^*\right)\mathscr{J}\hat{h}_{n\omega} + i\mathscr{C}\left(\bar{g}_{n\omega}\right) \tag{2}$$

The complex frequency $\omega = \hat{\omega}_\mathrm{r} + i\hat{\gamma}$ contains the real mode frequency $\hat{\omega}_\mathrm{r}$ and the mode growth rate $\hat{\gamma}$. Furthermore, $\mathscr{J}$ is the gyroaverage operator, $\mathscr{C}$ is a linearized Fokker-Planck electron-ion pitch-angle scattering collision operator, and

$$\omega^* = \omega_T^* \left(\frac{1}{\eta_e} + \zeta^2 - \frac{3}{2} \right). \tag{3}$$

is the kinetic diamagnetic frequency, with $\zeta = v/v_\mathrm{Th,e}$ and

$$\omega_T^* = \frac{k_\theta \rho_\mathrm{i}}{2} \sqrt{\frac{m_\mathrm{e}}{m_\mathrm{i}}} \frac{v_\mathrm{Th,e}}{R} \frac{R}{L_{T_e}} \tag{4}$$

where $\mathrm{v_{Th,e}} = \sqrt{\mathrm{2T_e/m_e}}$ is the electron thermal velocity. $L_{T\mathrm{e}}$ is the electron temperature scale length. The electron and ion mass and temperature are denoted m_e, m_i, T_e, and T_i, respectively. ρ_i is the ion Larmor radius and R the major radius.

The linear dispersion equation for MT modes can be obtained by solving Ampère's law and the Poisson equation written in variational form. One important property of Lagrangian $\mathscr{L}$ is that it vanishes when ϕ and $A_\parallel$ match the solution of Maxwell's equations

$$\mathscr{L} = -\frac{1}{\mu_0} \int d^3\mathbf{x} \left| \nabla_\perp A_\parallel \right|^2 + \int d^3\mathbf{x} (J_\parallel A_\parallel^* - \rho \phi^*), \tag{5}$$

where ρ is the charge density. The complex conjugate of the electric potential and the vector potential are denoted ϕ^* and $A_\parallel^*$, respectively. Next, this functional will be related to quasilinear fluxes. This allows deriving predictions of the turbulent fluxes produced by MT turbulence.

B. Stochasticity and magnetic transport

Nonlinear gyrokinetic simulations have been performed in order to compute the characteristics of MT turbulence and the associated heat fluxes in tokamak plasmas, identifying as a key characteristic that MT turbulence produces a substantial electron heat flux due to flutter motion along perturbed field lines[8,9,62,65,67]. A Rechester-Rosenbluth[67] -based reduced model for such transport driven by MT turbulence is detailed here and compared with nonlinear simulations. One important step is to establish the conditions under which a set of magnetic perturbations induces transport. It can be anticipated[8,9] that electrons are mostly affected by magnetic turbulent fluctuations.

Consider a magnetic fluctuation, which derive from a perturbed vector potential that can be written as a Fourier series

$$\tilde{A}_\parallel(r,\theta,\varphi,t) = \sum_{m,n,\omega} \tilde{A}_{\parallel,mn\omega}(r) \mathrm{e}^{i(m\theta + n\varphi - \omega t)}. \tag{6}$$

For a given level of magnetic fluctuations $\tilde{B}_r/B_{eq}$, where $\tilde{B}_r$ is the radial component of the perturbed magnetic field and B_{eq} the equilibrium field, the effective radial velocity of a particle that closely follows a field line is $(\tilde{B}_r/B_\mathrm{eq})v_\parallel$. A simple random-walk argument predicts a diffusion coefficient $\mathrm{D_M}$ of the order on $D_\mathrm{M} \sim \tilde{b}_r^2 \mathrm{v}_\parallel^2 \tau_\mathrm{c}$, where τ_c is a correlation time and

$$\tilde{b}_r = \left\langle \left(\frac{\tilde{B}_r}{B_\mathrm{eq}} \right)^2 \right\rangle^{1/2} \tag{7}$$

is the root-mean-square of the radial magnetic fluctuations (the outer bracket designates a statistical average over time and space). Hence, the diffusion coefficient increases with the parallel velocity unless the correlation time decreases more quickly with velocity. In fact, a reasonable estimate of τ_c is $L_{\parallel\mathrm{c}}/\left|v_\parallel\right|$, where $L_{\parallel\mathrm{c}} = 2\pi q R_0$ is the parallel correlation length of the perturbed magnetic field. The diffusion coefficient then becomes

$$D_\mathrm{M} \sim \tilde{b}_r^2 L_{\parallel\mathrm{c}} \left| v_\parallel \right| \tag{8}$$

This is the well-known Rechester-Rosenbluth expression[67,68], which later was found to describe the transport due to MT turbulence[32,70].

Electrons diffuse much more quickly than ions since the ratio of electron to ion thermal velocities scales as $\sqrt{m_\mathrm{i}/m_\mathrm{e}}\sqrt{T_\mathrm{e}/T_\mathrm{i}} \gg 1$. This leads to charge separation and to a positive radial electric field is in the turbulence frame of reference, i.e., the frame of reference that moves with a velocity equal to the mean phase velocity of the fluctuations. In the laboratory frame, this effect materializes through a rotation of fluctuations in the electron diamagnetic direction.

There is no requirement for the heat flux to vanish. Field-line diffusion produces mainly an electron heat flux. For the cases discussed here, MT turbulence is found to produce a finite electric potential, as does the linear MT mode. Therefore, substantial particle and ion heat fluxes are also possible, but dominantly due to $E \times B$ drift velocity fluctuations. In reality, however, MT turbulence tends not to produce any appreciable electrostatic flux, as the corresponding phase relations produce no contribution to the instability.

III. MICROTEARING TURBULENCE

This section compares analytical predictions with direct numerical simulations of microtearing turbulence. As per Eq. (8), the diffusion coefficient, based on a Rechester-Rosenbluth (RR) reduced model, scales as the square of the level of magnetic fluctuations. Since the electron thermal diffusivity can be approximated by the RR coefficient based on the field-line diffusion coefficient multiplied by a thermal velocity, it is expected that a gyrokinetically computed diffusivity should obey the same scaling. In Ref.[31], it was seen that linear MT growth rates are boosted by the magnetic drift and perturbed electric potential. A simple mixing-length argument then implies that the level of fluctuations, and the electron heat flux, will be reduced

PLEASE CITE THIS ARTICLE AS DOI: 10.1063/5.0104879

when switching off curvature and electric potential in nonlinear MT simulations.

Table I: Physical input parameters used for gyrokinetic simulations.

ε	s_0	$\beta(\%)$	R/L$_{Te}$	R/L$_{Ti}$	R/L$_{ne}$	q	$\nu_{\mathrm{ei}}^{\mathrm{GKW}}$	T$_\mathrm{e}$/T$_\mathrm{i}$
0.22	1.1	1.55	8	0	0.3	1.3	0.02	1

For the gyrokinetic simulations on which this paper is based, the Miller parametrisation[30] interface is used. For this case, a circular plasma with an elongation $\kappa = 1$, a triangularity $\delta = 0$ and the parameters given in Tab. I are used. These values were arbitrarily chosen to have a sufficiently high MT growth rate at high collisionality. The ion temperature gradient is set to 0, in order to supress ITG modes. It is important to note that the ion temperature gradient was set to zero to avoid multi-mode drive. Figure 1 shows the linear growth rate of MT modes as a function of $k_\theta \rho_\mathrm{i}$. For each point in Fig. 1, the eigenfunction of the modes is inspected. MT modes are the dominant instability for $k_\theta \rho_\mathrm{i}$ ranging from 0.04 to 1.0. As a representative example, Fig. 2 shows the perturbed vector potential and electric potential along the magnetic field line at $k_\theta \rho_\mathrm{i} = 0.3$, using the ballooning representation[21]. Note that moderate scale disparity is observed between the potentials, akin to, what was observed in Ref.[50].

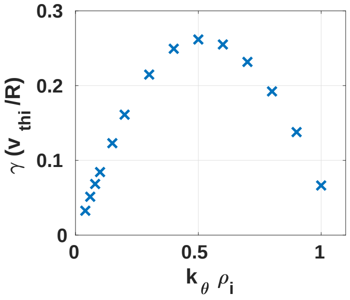

Figure 1: The linear growth rate of microtearing modes as a function of the normalized poloidal wavenumber $k_\theta \rho_i$.

Figure 3 shows the perturbed vector potential and kinetic conductivity in real space as functions of the radial coordinate x at $k_\theta \rho_\mathrm{i} = 0.3$ for $\nu_{\mathrm{ei}}^{\mathrm{GKW}} = 0.02$ (blue curve) and $\nu_{\mathrm{ei}}^{\mathrm{GKW}} = 0.8$ (red curve). The x coordinate is defined as the distance from the resonant flux surface, normalized to the thermal ion Larmor radius as: $x = (r - r_0)/\rho_i$. The kinetic conductivity σ_0 is defined as the ratio of the parallel current , $\tilde{J}_\parallel$ to the perturbed electric field. The parallel electric fields is defined as:

$$\tilde{E}_\parallel = -\frac{\partial \tilde{A}_\parallel}{\partial t} - \nabla_\parallel \tilde{\phi}, \tag{9}$$

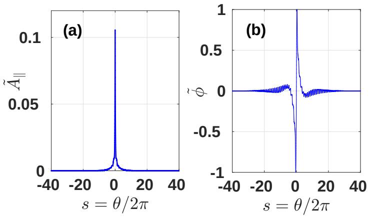

Figure 2: (a) Real part of the perturbed vector potential and (b) of the electric potential along the magnetic field line at $k_\theta \rho_\mathrm{i} = 0.3$ and $\nu_{\mathrm{ei}}^{\mathrm{GKW}} = 0.02$.

Using Eq. (9), the perturbed parallel current can be written as:

$$\tilde{J}_\parallel = \sigma_0 \Big(-\frac{\partial \tilde{A}_\parallel}{\partial t} - \nabla_\parallel \tilde{\phi} \Big) = +i\omega\sigma_0 \Big(\tilde{A}_\parallel - \frac{k_\parallel}{\omega} \tilde{\phi} \Big) = i\omega\sigma_0 a_\parallel, \tag{10}$$

where $a_\parallel$ is defined as:

$$a_\parallel = \tilde{A}_\parallel - \frac{k_\parallel}{\omega} \tilde{\phi}. \tag{11}$$

The perturbed kinetic conductivity σ plays an important role in stability. One may gain a more intuitive understanding by starting with a slab description of the current sheet around a resonant surface, where $q = m/n$, m and n are the poloidal and toroidal mode numbers, respectively. Ampère's Law is solved in two distinct regions, the outer and the inner region. Outside the resonant surface there is no current leading to $\nabla^2 \hat{A}_\parallel = 0$, and inside the resonant surface $\nabla^2 \hat{A}_\parallel = -\mu_o \hat{J}_\parallel$. The parity of the (m, n) eigenfunction is even, in the outer region $A_\parallel$ decay as $\exp(-|k_\theta||x|)$ whereas in the inner region the current sheet is thin, and $A_\parallel$ varies slowly, consistently with a constant-$A_\parallel$ approximation[51]. The development of an analytical calculation for MT is challenging, it is common to use the constant-$A_\parallel$ approximation in order to derive the dispersion relation. Ref.[19] describes in detail the domain where the constant-$A_\parallel$ approximation is valid. $A_\parallel$ is assumed to be constant across the current layer with $J_\parallel$ producing a jump in $dA_\parallel/dx$ across the layer. This approximation is valid under the condition[19]:

$$\eta_e^2 |\beta (L_s/L_n)^2| \ll 1 \tag{12}$$

where $L_s = qR/s_0$, and with the set of parameters chosen (see Tab.I) the constant-$A_\parallel$ approximation is valid. The matching of the internal and external solutions in physical space is achieved by integrating the Ampère equation radially,

$$\lim_{L\to 0} \frac{1}{A_\parallel(0)} \frac{dA_\parallel}{dx}\Big|_{-L}^{L} = -\int_{-\infty}^{+\infty} \sigma(x) dx \tag{13}$$

where $\sigma(x)$ is the perturbed conductivity defined as the ratio between the parallel current density with the perturbed parallel vector potential:

$$\sigma(x) = \frac{\tilde{J}_{\parallel}}{\tilde{A}_{\parallel}} \tag{14}$$

with $\tilde{J}_{\parallel} = i\omega\sigma_0 a_{\parallel}$ [see Eq. (10)] thus implying that

$$\sigma(x) = i\omega\sigma_0\left(1 - \frac{k_{\parallel}}{\omega}\frac{\tilde{\phi}}{\tilde{A}_{\parallel}}\right) \tag{15}$$

L is chosen such that:

$$\delta_J = \frac{L_s}{L_{T_e}}\rho_e\sqrt{\frac{\nu_{ei}}{\omega^*}} \ll L \ll \frac{1}{|k_\theta|}, \tag{16}$$

and with δ_J defined as the width of the current sheet, $L_s = qR/s$ the magnetic shear length, s the magnetic shear, L_{T_e} the electron temperature gradient length scale, ρ_e is the electron Larmor radius, ω^* the kinetic diamagnetic frequency, ν_{ei} the collisional frequency and k_θ is the poloidal mode number. For MT, the parameter Δ' can be defined as:

$$\Delta' = \lim_{L\to 0}\frac{1}{A_{\parallel}(0)}\frac{dA_{\parallel}}{dx}\Big|_{-L}^{L} = -2|k_\theta|, \tag{17}$$

The final matching condition gives

$$2|k_\theta| = \int_{-\infty}^{+\infty}\sigma(x)dx. \tag{18}$$

The kinetic conductivity $\sigma(x)$ is written using the Fourier decomposition, composed by a real part and complex part. Regarding Eq. (18), $Re(\sigma) > 0$ is consistent with $|k_\theta| > 0$. Ref.[70] discusses the effect of a wide range of physical plasma parameters on the microtearing current layer.

The electron and ion inertial length are defined as:

$$\lambda_s = \frac{c}{\omega_{ps}} \tag{19}$$

where s indicates the charged particles species considered ($s = e, i$ for electrons and ions) and ω_{ps} is defined as

$$\omega_{ps} = \left(\frac{4\pi n_s e^2}{m_s}\right)^{1/2} \tag{20}$$

One can note that the relation between the electron and ion skin depth is given by:

$$\lambda_e = \sqrt{\frac{m_e}{m_i}}\lambda_i \tag{21}$$

and the ion Larmor radius can be written as the function of the ions skin depth:

$$\rho_i = \sqrt{\frac{\beta}{2}}\lambda_i \tag{22}$$

Note that the electron skin depth

$$\frac{\lambda_e}{\rho_s} = \left(\frac{2}{\beta}\frac{m_e}{m_i}\right)^{1/2} \approx 0.17\ . \tag{23}$$

Given that the current layer in the present simulations is on the order of $0.1 - 0.2\rho_s$, this value is consistent with the usual tearing physics set by the electron skin depth.

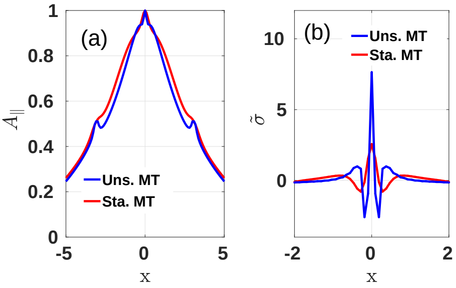

Figure 3: Real part (a) of perturbed vector potential in real space. (b): the linear perturbed kinetic conductivity σ in real space, for stable (red: $\nu_{\rm ei}^{\rm GKW} = 0.8$, Pfirsch-Schlüter regime) and unstable (blue: $\nu_{\rm ei}^{\rm GKW} = 0.02$, banana regime) MT modes, both for $k_\theta\rho_{\rm i} = 0.3$

Figure 3 shows the radial kinetic conductivity σ for MT modes at different collisionality regimes, banana regime (blue curve: $\nu_{\rm ei}^{\rm GKW} = 0.02$) and Pfirsch-Schlüter regime (red curve: $\nu_{\rm ei}^{\rm GKW} = 0.8$, and for $k_\theta\rho_{\rm i} = 0.3$. The kinetic conductivity σ is localized around the resonant surface. The calculation of the positive and negative areas of the perturbed kinetic conductivity shows that the positive parts dominate when MT are unstable. When the positive part of the perturbed kinetic conductivity is eroded MT become stable. It is therefore informative to compute the radial profile of σ near a resonant surface, to identify a potential nonlinear saturation mechanism based on a modification of the relative weights of positive and negative values of the conductivity. The structure of the perturbed kinetic conductivity will be analyzed in nonlinear simulations.

Based on these linear microtearing results, numerical settings for nonlinear gyrokinetic simulations are chosen as listed in Tab. II.

Table II: Numerical input parameters used for nonlinear gyrokinetic simulations. N_s is the number of grid points along the field line per poloidal turn, N_μ is the number of magnetic moment grid points, $N_{v_\parallel}$ is the number of parallel velocity grid points, N_x is the number of modes in the radial direction, and L_x and L_y the radial and binormal box sizes.

$\mathbf{N}_\mu$	$\mathbf{N}_{\mathrm{v}_\parallel}$	$\mathbf{N}_{\mathrm{s}}$	$\mathbf{N}_{\mathrm{x}}$	L_x	L_y

16	30	40	679	150	157

Based on the parameters presented in Tab. I and in Tab. II, a set of nonlinear gyrokinetic simulations has been conducted, ensuring numerical convergence, using the GKW code[30]. The radial wave number $\mathrm{k_r}\rho_\mathrm{i}$ covers the range $[-10, 10]$, and the finite $k_\theta\rho_\mathrm{i}$ ranges from 0.04 to 1.2. Figs.4-a and 4-b show the $A_\parallel$ and ϕ spectra, respectively, averaged over the quasi-stationary state.

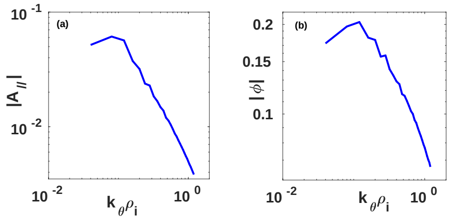

Figure 4: Binormal spectra from the reference case, with zonal flow and zonal fields. (a) $|A_\parallel|$ and (b) ϕ spectra.

One key question concerns how the magnetic fluctuation level in Eq. (7) is linked to the associated transport. The electron heat diffusivity χ_e^{em} can be expressed in terms of the electron heat flux due to the magnetic flutter

$$\mathrm{Q_e^{em}} = -n_\mathrm{e}\chi_\mathrm{e}^\mathrm{em}\nabla\mathrm{T_e}. \tag{24}$$

Thus,

$$\chi_\mathrm{e}^\mathrm{em} = \frac{R\mathrm{Q_e^{em}}}{n_\mathrm{e}T_\mathrm{e}R/L_{\mathrm{T_e}}} = R\rho_*^2 v_\mathrm{Th,i}\frac{\mathrm{Q}_{em}^\mathrm{GKW}}{R/\mathrm{L_{T_e}}} \tag{25}$$

where $\mathrm{Q_{em}^{GKW}}$ is the magnetic flutter component of the normalized heat flux[30]. The magnetic heat flux $\mathrm{Q_{em}^{GKW}}$ is determined by nonlinear GKW simulations. Figure 5 shows the electron heat diffusivity $\chi_\mathrm{e}(Rv_\mathrm{Th,i}\rho_*^2)$ as a function of the magnetic fluctuation level $(\tilde{b}_r/\rho_*)^2$ for three values of the electron temperature gradient. Effectively the magnetic field fluctuation amplitude increases with R/L_{T_e}, and the heat diffusivity is proportional to b_r^2.

One can now compare the diffusion coefficient

$$D_M = \tilde{b}_r^2 L_{\parallel\mathrm{c}} v_{th_e} = \pi q R\tilde{b}_r^2 v_{th_e} \tag{26}$$

based on the RR reduced model[67]. The amplitude of the magnetic fluctuation level b_r is taken from nonlinear GKW simulations.

Figure 6 shows the electron heat diffusivity based on the RR reduced model as per Eq. (26) as a function of the electron heat diffusivity χ_e^{em} computed by GKW for the same three electron temperature gradients. The turbulent diffusivity is well-described by the RR reduced model.

Figure. 7 shows the radial profiles of (a) the vector potential and (b) the conductivity for $k_y = 0.12$. The vector potential has even parity and exhibits a shape similar to the one found in the linear stability analysis.

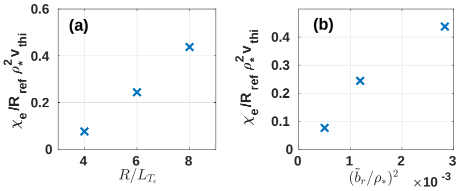

Figure 5: The electron heat diffusivity χ_e^{em} due to magnetic flutter (a) as a function of the electron temperature gradient R/L_{T_e} and (b) as a function of the magnetic fluctuation level.

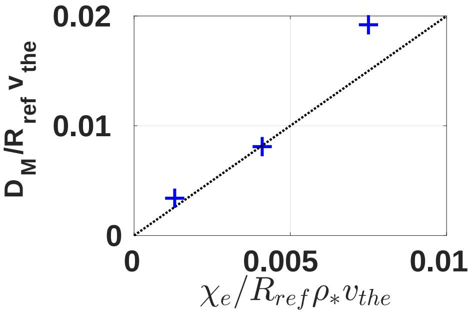

Figure 6: The electron heat diffusivity $D_\mathrm{M} = \pi qR\tilde{b}_r^2$, based on a Rechester-Rosenbluth reduced model as a function of the electron heat diffusivity χ_e^{em} computed by GKW

.

The conductivity is positive, consistent with a MT mode that is fed by the free energy available in the current layer. In Ref.[69], linear and nonlinear parity conservation are discussed. In electromagnetic gyrokinetic calculations, the parity of the perturbation is important because it is directly related to stochastization of the surface and stochastization of the surface occurs, when the perturbation has the tearing parity and the integral of $A_\parallel$ along the field line does not vanish. Linearly the parity of the mode is conserved but nonlinearly in the gyrokinetic equation the parities are mixed and no mixing would occur if no even parity is seeded. The parity mixture is important for generating magnetic disturbance which violates the magnetic surface.

Similarly to the linear regime, Fig. 3, non-linearly the negative tail of the conductivity far away from the resonant surface has been eroded relative to that in the central region. A positive conductivity is consistent with a nonlinear state where a negative conductivity is balanced by the cur-

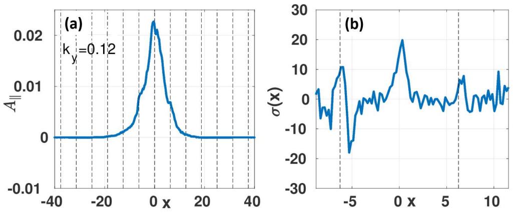

Figure 7: Amplitudes (a) of the perturbed vector potential and (b) of the kinetic conductivity σ in real space for $\mathrm{k_y} = 0.12$ for nonlinear runs. Dashed lines indicate resonant surfaces.

rent sheet response for the most unstable mode as

$$2|k_\theta| = \mu_0 \int_{-\infty}^{+\infty} \mathrm{d}x \sigma(x). \qquad (27)$$

Then, the effect of the electric potential on linear physics is investigated. Figure 8 shows the linear growth rates of MT modes as functions of $k_\theta \rho_\mathrm{i}$ for three different temperature gradients for the set of parameters listed in Tab. I.

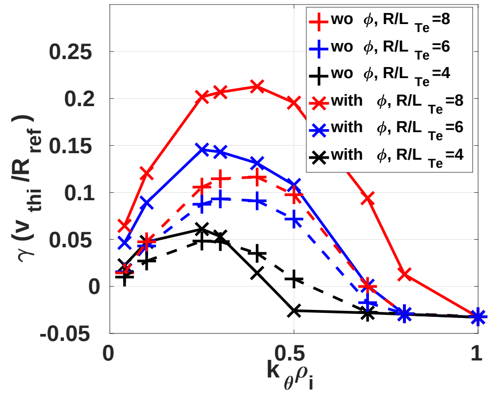

Figure 8: Linear growth rates as functions of the normalized wave number, $k_\theta \rho_i$ for three different temperature gradients. Dashed curves are obtained by switching -off the electric potential, whereas for the solid curves the electric potential is included.

Dashed curves are obtained by switching off the electric potential in GKW, whereas for the solid curves the electric potential is evolved self-consistently. MT modes are the dominant linear instability both with and without the inclusion of the electric potential.

IV. EFFECT OF THE ELECTRIC POTENTIAL IN SATURATION

In the previous section, the objective was to evaluate the role played by the electric potential on the microtearing modes destabilization. Clearly, the electric potential plays an important role, allowing a considerable increase on the MT growth rate. This raises the question of its role non -linearly, and whether the electric potential affects the MT saturation.

A second objective is to learn more about MT saturation, by removing step-by-step, the electric potential and the effect of zonal fields and zonal flows.

Zonal flows (ZFs) are $n = 0$, $m = 0$ electric field fluctuations at a finite radial wavenumber q_r. Zonal flows are well-known to regulate turbulent energy transfer in various turbulence regimes[58,59,71].

As will be shown here, for the present MT scenario, the electron heat transport increases when the electric potential is switched off. The study will now focus on impact of ϕ nonlinearly.

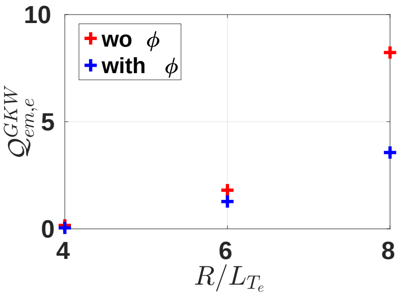

Figure 9: Magnetic flutter component of the electron heat flux $\mathrm{Q_{em,e}}$ with (blue) and without electric (red) as a function of the electron temperature gradient.

Figure 9 shows the magnetic flutter component of the electron heat flux $\mathrm{Q}_{em,e}$ as a function of the electron temperature gradient. To obtain the red points, the electric potential was switched off in GKW. Conversely, to obtain the blue points, the electric potential is included self-consistently. The transport is almost entirely driven by the magnetic fluctuations as is common for MT turbulence[8].

The magnetic flutter component of the electron heat fluxes increases with the electron temperature gradient. Figure 9 yields an interesting and unexpected result. The electron heat flux increases when the electric potential is switched off. The converse was expected on the basis of linear stability analysis. Hence, the perturbed electric potential plays an important regulating role in MT turbulence beyond its impact on the linear stability.

Figure 10 contains the normalized linear electron heat

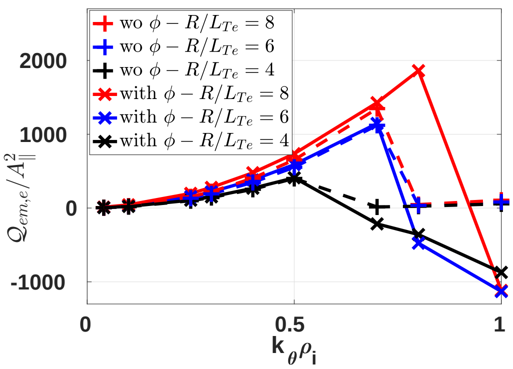

Figure 10: Normalized linear heat fluxes as functions of $k_\theta \rho_i$ with (solid curves) and without (dashed curves) the electric potential for three electron temperature gradients, $R/L_{Te} = 8.0$ (red), $R/L_{Te} = 6$ (blue) and $R/L_{Te} = 4$ (black).

fluxes as function of $k_\theta \rho_i$ with (solid curves) and without (dashed curves) the electric potential for different temperature gradients, as in Fig. 8. In GKW, the fluxes are normalized to $|\phi(s,t)|^2 + |A_\parallel(s,t)|^2$, where s is the coordinate along the magnetic field line. The normalized electron heat flux increases with the electron temperature gradient both with and without the electric potential. Thus, the normalized linear electron heat fluxes are comparable with and without the electric potential . This suggest that the effect observed on the electron heat fluxes nonlinearly is related to the amplitude of $A_\parallel$ and not due to a change in phase difference between $Q_{em,e}$ and $A_\parallel$.

Figure 11 represents a comparison between the quasilinear electron heat diffusivity in Eq. (26) with and without the electric potential for three values of the electron temperature gradient using the value of b_r^2 obtained in the nonlinear GKW simulations. The diffusivity calculated by GKW is well described by the Rechester-Rosenbluth quasi-linear diffusivity coefficient with and without the electric potential. However, it is important to note, as shown in the Ref.[32], this model breaks down when the fluctuation amplitudes become small, which, however, does not occur in the present case.

A primary candidate to explain the mismatch between linear and nonlinear response to ϕ are ZFs. ZFs are known to regulate the turbulent transport driven by electrostatic drift-wave instabilities. In this regard, MT turbulence regimes have received much less attention. However, as an analysis of MT turbulence in the H-mode pedestal indicates, the zonal mode can play an important role in saturation, although in that case the zonal $A_\parallel$ (commonly referred to as the zonal field) was responsible for the observed effect, whereas the ZF has little impact except on ETG scales.

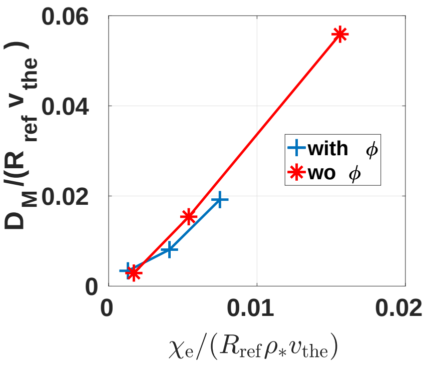

Figure 11: The quasilinear electron heat diffusivity $D_M = \pi q R \tilde{b}_r^2$ as a function of the electron heat diffusivity χ_e.

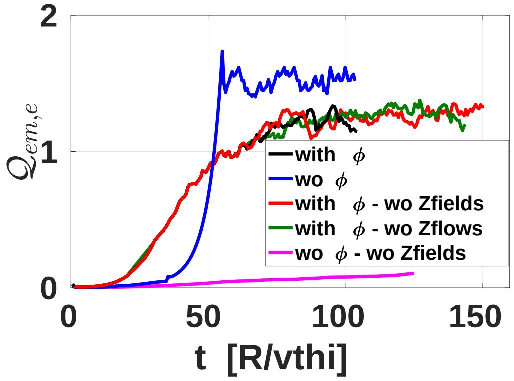

Figure 12: Time evolution of the magnetic flutter component of the electron heat fluxes ($Q_{em,e}$) for different cases: Black line: with ϕ; blue line: without ϕ; red line: with ϕ, with zonal flows and without zonal fields; green line: with ϕ, with zonal field and without zonal flow; pink line: without ϕ and without zonal field.

Figure 12 shows the time evolution of the magnetic flutter fluxes for different cases. Zonal flows and zonal fields have been suppressed artificially in GKW by suppressing the non-linear interactions in which ky=0 modes are involved. In practice, this means that non-linear interactions can excite ZFs but that ZFs do not interact non-linearly with other modes.

The black curve is the reference case, with ϕ and with zonal fields included. To obtain the blue curve, the electric potential was removed. When ϕ is switched off, the transport is higher. To obtain the green and red curves, zonal fields and zonal flows were deleted.

In the nonlinear simulations, when ϕ evolved self-consistently, little change is observed. Otherwise, when the zonal field and the electric potential are removed, see the pink curve on the Fig. 12, the flux drop considerably in comparison with the blue curve in the same figure.

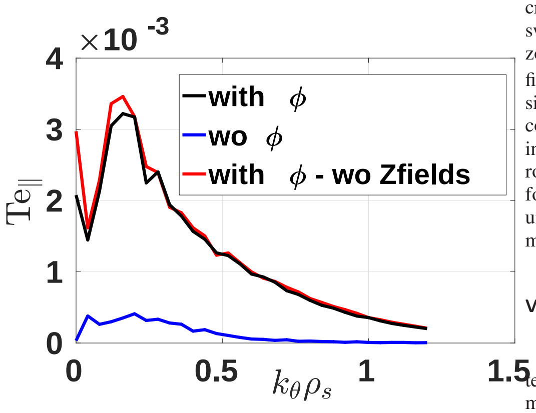

Figure 13: The parallel perturbed electron temperature as function of $k_\theta \rho_s$ for different cases. Black line: with ϕ; blue line: without ϕ; red line: with ϕ, with zonal flows and without zonal fields.

Thus, the following physical picture emerges for the present MT scenario. When the turbulence is driven by the self-consistent MT mode, i.e., with ϕ included, saturation is independent of the zonal flow or the zonal field, and instead relies on different processes. It has recently been demonstrated[75] that MT turbulence can saturate via (zonal) $T_{e,\|}$ corrugations (see also Refs.[76,77]); in that work, when deleting $T_{e,\|}^{zonal}$, fluxes increase substantially (while deleting ϕ^{zonal} or $A_{\|}^{zonal}$ produces only a small increase), as the system has to rely on another, less efficient saturation mechanism. As explained in Ref.[75], as the electrons move rapidly along the perturbed magnetic field associated with the islands in the low-order mode resonant surfaces, they also experience localized radial spreading. This leads to a short-circuiting of the perturbed T_e profile, leading to its flattening, thus lowering the effective temperature gradient that provides energy for the mode.

The paper hypothesizes that in different parameter regimes, different MT saturation mechanisms will be active. In the present case, as the electrostatic potential is removed, not only is the linear drive adjusted as per Fig. 1, but the saturation mechanism also changes, leading to higher heat fluxes. Confirming this interpretation, Fig. 13 shows the parallel perturbed electron temperature as a function of k_θ. A comparison between the black and red curves, both including ϕ but with vs. without zonal fields, respectively, shows little difference, showing that the default scenario, which is not sensitive to zonal-field removal, has substantial zonal $T_{e,\|}$. Conversely, comparing the blue and black curves, with and without ϕ, respectively, a substantial reduction in zonal $T_{e,\|}$ is seen, while fluxes (see Fig. 12) increase moderately. Thus, in the absence of ϕ, the system switches to a different, less efficient saturation mechanism: zonal fields and/or flows. The $T_{e,\|}^{zonal}$ mechanism is less efficient or possibly disabled when deleting ϕ, which is plausible, as building up a zonal temperature requires nonlinear coupling through ϕ and/or $A_{\|}$. Detailed studies are on going using JET experimental data to better understand the role played the electric potential and related consequences for saturation mechanisms, and to obtain a more thorough understanding in which parameter regions one saturation mechanisms or another is expected to be active.

V. CONCLUSIONS

The microtearing instability, which draws on the electron temperature gradient as a free-energy source and rearranges magnetic topology through the creation ion-Larmor-radius-scale magnetic islands, can be an important source of electron heat transport in fusion devices. Since its discovery in 1975, several analytical theories of MT have been developed, commonly neglecting key effects such as magnetic drifts, electric potential, or collisions. Here, based on the more encompassing model presented in Ref.[31], predictions of MT transport in tokamak plasmas are compiled and compared against direct nonlinear simulations with the GKW code. In agreement with findings reported by other groups, the quasilinear approach captures important nonlinear trends, e.g., confirming the diffusive nature and scalings of the magnetic flutter transport. It has been shown that the Rechester-Rosenbluth model is a good model for the prediction of electron heat diffusivity by microtearing turbulence.

However, a key difference is observed when artificially removing the electrostatic potential from simulations. In the linear case, MT growth rates and quasilinear fluxes are lowered by this procedure, whereas nonlinear heat fluxes increase. While further research into this effect is required, the data points to a change in saturation mechanism or, equivalently, a transition to a different MT turbulence regime. Upon ϕ removal, the original insensitivity to zonal flows and zonal fields appears to give way to a reliance on zonal-field saturation, albeit at a lower efficiency, leading to higher heat fluxes.

ACKNOWLEDGMENTS

This work has been carried out within the framework of the EUROfusion Consortium, funded by the European

Union via the Euratom Research and Training Programme (Grant Agreement No 101052200 — EUROfusion). Views and opinions expressed are however those of the author(s) only and do not necessarily reflect those of the European Union or the European Commission. Neither the European Union nor the European Commission can be held responsible for them.

This work was performed by using computational resources provided by the MARCONI-FUSION HPC.

DATA AVAILABILITY

The data that support the findings of this study are available from the corresponding author upon reasonable request.

REFERENCES

[1] The ASDEX Upgrade Team, *Nucl. Fusion* **29** (1980)
[2] F. Wagner, G. Becker, K. Behringer, D. Campbell, A. Eberhagen, W. Engelhardt, G. Fussmann, O. Gehre, J. Gernhardt, G. V. Gierke *et al.* *Phys. Rev. Lett.* **49**, 1408 (1982)
[3] D. R. Hatch1, C. Michoski, D. Kuang, B. Chapman-Oplopoiou, M. Curie, M. Halfmoon, E. Hassan, M. Kotschenreuther, S. M. Mahajan, G. Merlo, M. J. Pueschel, J. Walker, and C. D. Stephens *Phys. Plasmas* , **29**: 062501, 2022.
[4] M.J. Pueschel, P.W. Terry, and D.R. Hatch *Phys. Plasmas* , **21**: 055901, 2014.
[5] F. Jenko, W. Dorland, M. Kotschenreuther, and B. N. Rogers *Phys. plasmas*, **7(5)**:1904–1910, 2000.
[6] Z. Lin, T. S. Hahm, W. W. Lee, W. M. Tang, and R. B. White, *Phys. Plamas*, **7**: 1857, 2000.
[7] D.R. Hatch , M. Kotschenreuther , S.M. Mahajan , M.J. Pueschel , C. Michoski , G. Merlo , E. Hassan , A.R. Field , L. Frassinetti , C. Giroud , J.C. Hillesheim , C.F. Maggi , C. Perez von Thun , C.M. Roach , S. Saarelma , D. Jarema , F. Jenko and JET Contributors, *Nuclear Fusion*, **61**: 036015, 2021.
[8] D.R. Hatch, M. Kotschenreuther, S.Mahajan, P. Valanju, F. Jenko, D. Told, T. Görler, S. Sareelma, *Nucl. Fusion*, **56**: 104003, 2016.
[9] D.R. Hatch, M. Kotschenreuther, S.Mahajan, P. Valanju, and X. Liu. *Nucl. Fusion*, **57(3)** :036020, 2017.
[10] D.R. Hatch, M. Kotschenreuther, S.M. Mahajan, G. Merlo, A.R. Field, C. Giroud, J.C. Hillesheim, C.F. Maggi, C. Perez von Thun, C.M. Roach, S. Saarelma, and JET Contributors. *Nucl. Fusion*, **59(8)**:086056, 2019.
[11] S. Moradi, I. Pusztai, W. Guttenfelder, T. Fulop, and A. Molln, *Nucl. Fusion*, **53**: 063025, 2013.
[12] B. Chapman-Oplopoiou, D.R. Hatch, A.R. Field, L. Frassinetti, J.C. Hillesheim, L. Horvath, C.F. Maggi, J.F. Parisi, C.M. Roach, S. Saarelma and J. Walker, *Nucl. Fusion*, **62**: 086028, 2022.
[13] Jason F. Parisi , Felix I. Parra , Colin M. Roach , Carine Giroud , William Dorl, , David R. Hatch , Michael Barnes , Jon C. Hillesheim , Nobuyuki Aiba , Justin Ball , Plamen G. Ivanov and JET contributors, *Nucl. Fusion*, **61**: 036015, 2021.
[14] W. Guttenfelder , R.J. Groebner , J.M. Canik , B.A. Grierson , E.A. Belli and J. Candy, *Nucl. Fusion*, **61**: 056005, 2021.
[15] P. B. Snyder, N. Aiba, M. Beurskens, R. J. Groebner, L. D. Horton, A. E. Hubbard, J. W. Hughes, G. T. A. Huysmans, Y. Kamada, A. Kirk, C.Konz, A. W. Leonard, J. Lonnroth, C. F. Maggi, R. Maingi, T. H. Osborne, N. Oyama, A. Pankin, S. Saarelma, G. Saibene, J. L. Terry, H. Urano, and H. R. Wilson, *Nucl. Fusion*, **49**: 085035, 2009.
[16] P.B. Snyder, T.H. Osborne, K.H. Burrell, *Phys. Plasmas* **19**, 056115 (2012).
[17] R. D. Hazeltine, D. Dobrott and T.S. Wang, *Phys. Fluids*, **18**:1778-1786, 1975.
[18] J.F. Drake and Y.C. Lee, *Phys. of Fluids*, **20**: 1341-1353, 1977.
[19] N. T. Gladd, J. F. Drake, C. L. Chang, and C. S. Liu *Phys. Fluids* **23**: 1182, 1990.
[20] P. J. Catto and M. Rosenbluth, *Phys. Fluids*, **24**: 243-255, 1981.
[21] J.W. Connor, and R.J. Hastie, *Physics of Fluids*, 1987.
[22] J.W. Connor, S.C. Cowley and R.J. Hastie, *Plasma Phys. Control. Fusion*, **32**: 799-817 (1990).
[23] A. I Smolyakov, *Sov. J. Plasma Phys.*, **15**: 1153-1159, 1989.
[24] X.Garbet, F. Mourgues, A. Samain *Plasma Phys. Control. Fusion*,**30**: 343-363, 1988.
[25] X.Garbet, F. Mourgues, A. Samain *Plasma Phys. Control. Fusion*, **32**: 131-140, 1990.
[26] A.Zocco, N. F.Loureiro, D. Dickinson, R. Numata and C.M. Roach *Plasma Phys. Control. Fusion*, **57**: 065008, 2015.
[27] J. L. Larakers, R. D. Hazeltine, and S. M. Mahajan. *Phys. Plasmas*, **27(6)**: :062503, 2020.
[28] M.Hamed, M.Muraglia,Y. Camenen, X. Garbet, *Contrib. Plasm. Phys.*, **58**: 529-533, 2018
[29] M. Hamed, M. Muraglia, Y. Camenen, X. Garbet, *J. Phys.: Conf. Ser.* **1125**: 012012, 2018
[30] A.G. Peeters, Y. Camenen, F.J. Casson, W.A. Hornsby, A.P. Snodin, D. Strintzi, and G. Szepesi, *Computer Physics Communication*, **180**: 2650, 2009.
[31] M. Hamed, M. Muraglia, Y. Camenen, X. Garbet a,d O. Agullo, *Phys. Plasmas*, **26**: 092506, 2019.
[32] H. Doerk, F. Jenko, T. Görler, D.Told, M.J. Pueschel, and D.R. Hatch *Phys. Plasmas*, **19**: 055907, 2012.
[33] D. Told, F. Jenko, P. Xanthopoulous, L.D. Horton, E. Wolfrum and ASDEX Upgrade Team, *Phys. Plasmas*, **15**: 102306, 2008.
[34] N. Ohyabu, G. Jahns, R. Stambaugh, and E. Strait, *Phys. Rev. Lett.* , **58**: 120, 1987.
[35] X. Jian, C. Holland, J. Candy, S. Ding E. Belli, V. Chan, G. M. Staebler, A. M. Garofalo, J. Mcclenaghan, and P. Snyder, *Phys. Plasmas*, **28**: 042501, 2021.
[36] O. Nelson, F. M. Laggner, A. Diallo, D. Smith, Z. A. Xing, R. Shousha, E. Kolemen, *Nucl. Fusion*, **61**: 116038, 2021.
[37] E. Hassan , D.R. Hatch , M.R. Halfmoon , M. Curie , M.T. Kotschenreuther , S.M. Mahajan , G. Merlo , R.J. Groebner , A.O. Nelson and A. Diallo, *Nucl. Fusion*, **62**: 026008, 2021.
[38] D.J Applegate, C. M. Roach, J. W. Connor, S. C. Dorland, R. J Hastie and N. Joiner, *Phys. Control. Fusion*, **49**: 1113, 2007.
[39] M. Kotschenreuther, W. Dorland, Q.P. Liu, M.C. Zarnstorff, R.L. Miller, Y.R. Lin-Liu, *Nucl. Fusion*, **40**: 677, 2000.
[40] M. Kotschenreuther, X. Liu, D.R. Hatch, S. Mahajan, L. Zheng, A. Diallo, R. Groebner, the DIIID TEAM, J.C. Hillesheim, C.F. Maggi, C. Giroud, F. Koechl, V. Parail, S. Saarelma, E. Solano, A. Chankin, and JET Contributors. *Nucl. Fusion*, **59(9)** :096001, 2019.
[41] K. Wong, S. Kaye, D. Mikkelsen, J. Krommes, K. Hill, R. Bell and B. LeBlank, *Phys. Rev. Lett*, **99**: 135003, 2007.
[42] H.R. Wilson, J.-W. Ahn, R.J. Akers, D. Applegate, R.A. Cairns, J.P. Christiansen, J.W. Connor, G. Counsell, A. Dnestrovskij, W.D. Dorland, M.J. Hole, N. Joiner, A. Kirk, P.J. Knight, C.N. Lashmore-Davies, K.G. McClements, D.E. McGregor, M.R. O'Brien, C.M. Roach, S. Tsaun, G.M. Voss, *Nucl. Fusion*, **44**: 917, 2004.
[43] W. Guttenfelder , J. Candy, S.M. Kaye, W.M. Nevins, R.E. Bell, G. W. Hammett, B. P. LeBlanc, and H. Yuh, *Phys. Plasmas*, **19**: 022506, 2012.
[44] C.M. Roach, D.J. Applegate, J.W. Connor, S.C. Cowley, W.D. Dorland, R.J. Hastie, N. Joiner, S. Saarelma, A.A. Schekochihin, R.J. Akers, C. Brickly, A.R. Field, M. Valovic, and the MAST team, *Plasma Phys. Control. Fusion*, **47**: 233, 2005.
[45] D.R. Smith, W. Guttenfelder, B.P. LeBlanc, D.R. Mikkelsen, *Plasma Phys. Control. Fusion*, **53**: 035013, 2011.
[46] D. Dickinson, C.M. Roach, S. Saarelma, R. Scannell, A. Kirk and H.R. Wilson, *Phys. Rev. Let.*, **108**: 135002, 2012.
[47] J. Chowdhury, Yang Chen, Weigang Wan, Scott E. Parker, W. Guttenfelder, and J. M. Canik. *Phys. plasmas*, **23(1)** :012513, 2016.
[48] Aditya K Swamy, R Ganesh, J Chowdhury, S Brunner, J Vaclavik, and L Villard., *Journal of Physics: Conference Series*, 561:012017, 2014.
[49] I. Predebon, F. Sattin, M.Veranda *Phys. Plasmas*, **20**: 040701, 2013.
[50] D. Carmody, M.J Pueschel, and P.W Terry *Phys. of Plasmas*, **20**: 052110, 2013.

[51] Fitzpatrick, R. J. Hastie, T. J. Martin, and C. M. Roach *Nucl. Fusion*, **33**: 1533, 1993.

[52] J. Citrin, C. Bourdelle, P. Cottier, D. F. Escande, Ö. D. Gürcan, D. R. Hatch, G. M. D. Hogeweij, F. Jenko, and M. J. Pueschel *Phys. Plasmas*, **111**: 062305 , 2012.

[53] A. Casati, C. Bourdelle, X. Garbet, F. Imbeaux, J. Candy,F. Clairet, G. Dif-Pradalier, G. Falchetto, T.Gerbaud,V. Grandgirard, O.D. G urcan, P. Hennequin, J. Kinsey,M. Ottaviani, R. Sabot, Y. Sarazin, L. Vermare, and R.E.Waltz *Nucl. Fus.*, **49(8)**: :085012, 2009.

[54] T. Rafiq, J. Weiland, A. H. Kritz, L. Luo, and A. Y. Pankin *Phys. Plasmas*, **23**: , 062507, 2016

[55] T. Xie, M. J. Pueschel, and D. R. Hatch *Phys. Plasmas*, **27**: 082306, 2020

[56] K. Itoh, S. -I. Itoh, P. H. Diamond, T. S. Hahm, A. Fujisawa, G. R. Tynan, M. Yagi, Y. Nagashima *Phys. Plamas*, **15**: 055502, 2006.

[57] B. N. Rogers, W. Dorland, and M. Kotschenreuther *Phys. Rev. Lett.*, **85**: 5336, 2000.

[58] D. R. Ernst, K. H. Burrell, W. Guttenfelder, T. L. Rhodes, A. M. Dimits, R. Bravenec, B. A. Grierson, C. Holland, J. Lohr, A. Marinoni, G. R. McKee, C. C. Petty, J. C. Rost, L. Schmitz, G. Wang, S. Zemedkun, L. Zeng, and the DIII-D Team *Physics of Plasmas*, **25(1)**: 012308, 2018.

[59] P. W. Terry, B. J. Faber, C.C. Hegna, V. Mirnov, M. J. Pueschel, G. G. Whelan *Phys. Plamas*, **25(1)**:012308, 2018.

[60] P.W. Terry, M.J. Pueschel, D. Carmody, and W.M. Nevins *Phys. Plamas*, **20**: 112502, 2014

[61] K.D. Makwana, P.W. Terry, M.J. Pueschel, and D.R. Hatch *Phys. Rev. Lett.*, **112**:095002, 2014.

[62] M. J. Pueschel, M. Kammerer, and F. Jenko *Phys. Plasmas*, **15**: 102310, 2008.

[63] F. Jenko and A. Kendl *Phys. Plasmas*, **9**: 4103, 2002.

[64] M. J. Pueschel, H. Doerk, T. Gorler, F. Jenko, *37th EPS Conference on Plama Physics* P1. 1081, 2013.

[65] M. J. Pueschel and F. Jenko *Phys. Plamas*, **17**: 062307, 2010.

[66] M.J. Pueschel, T. Dannert, and F. Jenko. *Computer Physics Communications*, **181(8)**:1428–1437, 2010.

[67] A. B. Rechester, M. N. Rosenbluth and R. B. White, *Phys. Rev. A*, **23** 2664–2672 (1981).

[68] A. B. Rechester, M. N. Rosenbluth *Phys. Rev. Lett.*, **40** 38-41 (1978).

[69] Ishizawa, Y. Kishimoto and Y. Nakamura , *Plasma Physics and Controlled Fusion*, **61**: 054006, 2019.

[70] H. Doerk, F. Jenko, M. J. Pueschel, and D. R. Hatch, *Phys. Rev. Lett.* , **106** 155003 (2011).

[71] P. H. Diamond, S. -I. Itoh, K. Itoh, and T. S. Hahm, *Phys. control. fusion*, **47**: R35, 2005.

[72] P.W. Terry, P.Y. Li, M.J. Pueschel, and G.G Whelan, *Phys. Rev. Lett.*, **126**: 025004, 2021.

[73] M.J. Pueschel, P.Y. Li and P.W. Terry, *Nucl. fus.*, **61**: 054003, 2021.

[74] P.Y. Li, P.W. Terry, G.G. Whelan, and, M.J. Pueschel, *Phys. Plasmas*, **28**: 102507, 2021.

[75] Ajay C.J., B. McMillan, and M.J. Pueschel, Microtearing turbulence saturation via electron temperature flattening at low-order rational surfaces, submitted.

[76] R. E. Waltz, *Phys. Plasmas*, **17**: 072501, 2010.

[77] M.J. Pueschel, T. Görler, F. Jenko, D.R. Hatch, A.J. Cianciara, *Phys. Plasmas*, **17**: 072501, 2010.

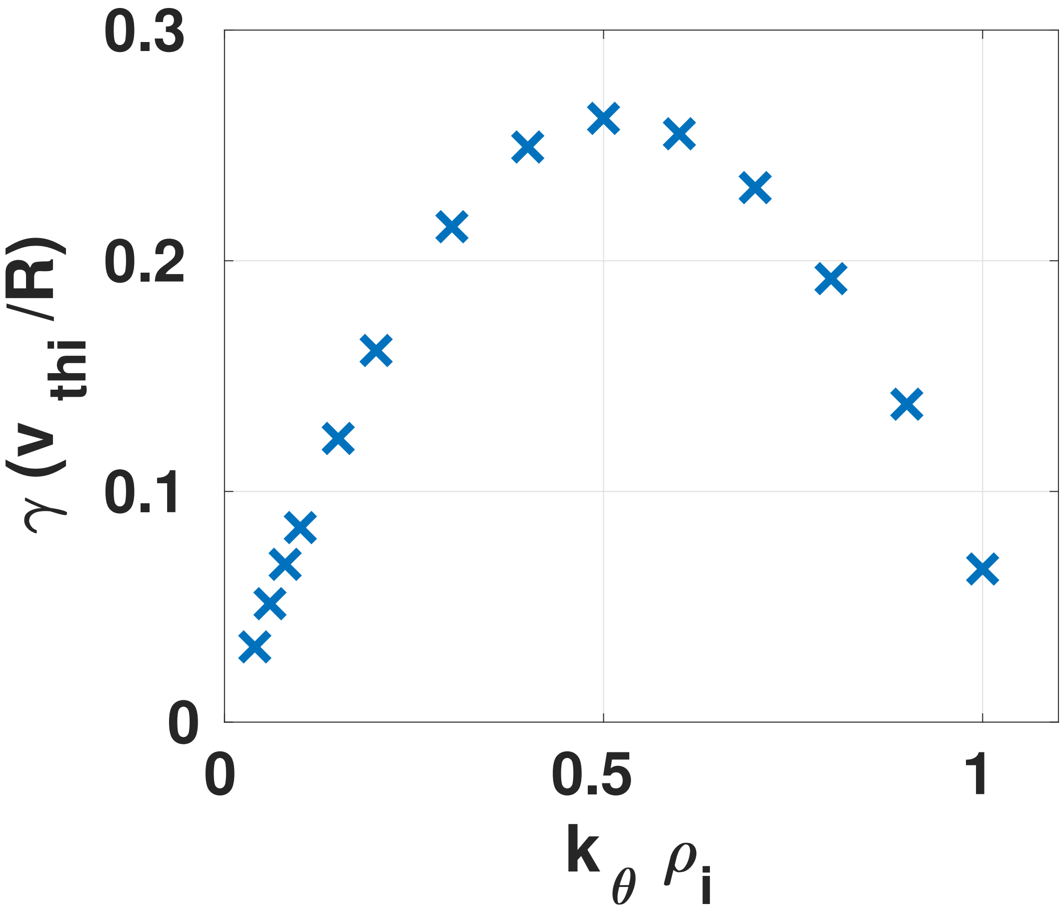
0.3
0.2
0.1
0
γ (v_thi /R)
0
0.5
1
k_θ ρ_i

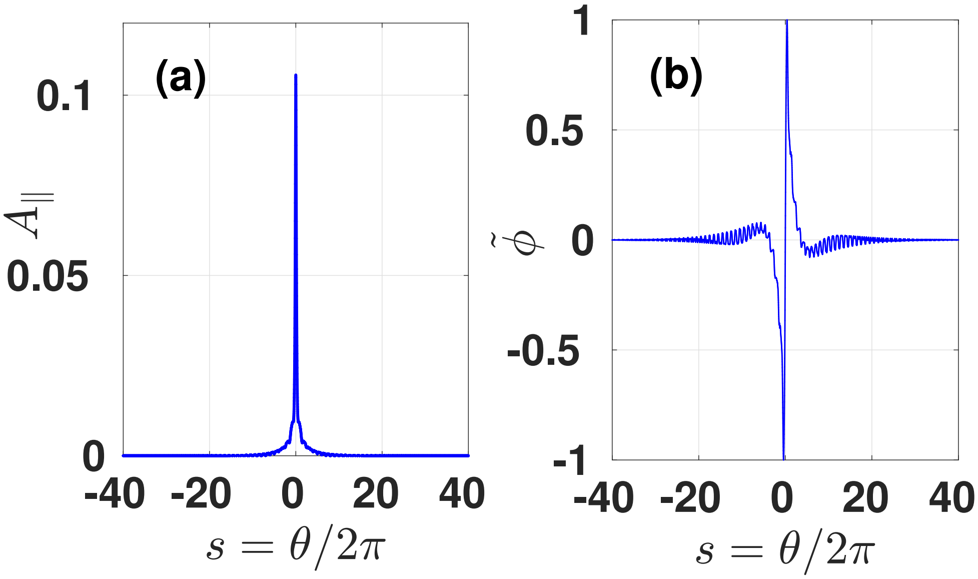
(a)
$\tilde{A}_{\|}$
0.1
0.05
0
-40
-20
0
20
40
$s = \theta/2\pi$
(b)
$\tilde{\phi}$
1
0.5
0
-0.5
-1
-40
-20
0
20
40
$s = \theta/2\pi$

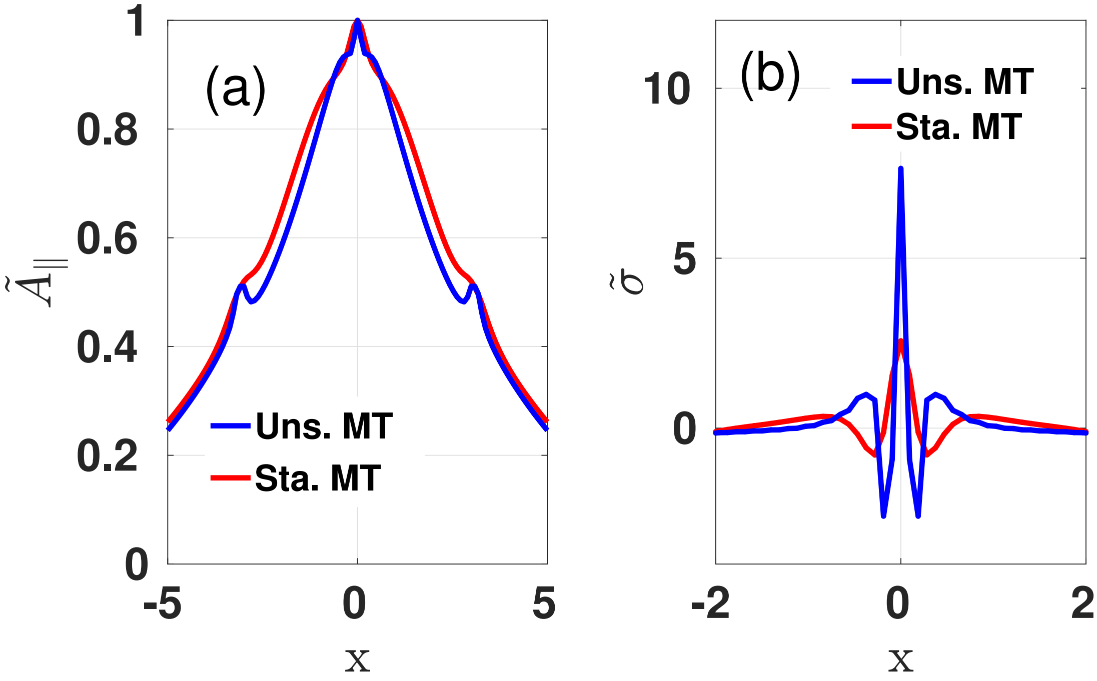
(a)
$\tilde{A}_{\|}$
1
0.8
0.6
0.4
0.2
0
-5
0
5
x
Uns. MT
Sta. MT
(b)
$\tilde{\sigma}$
10
5
0
-2
0
2
x
Uns. MT
Sta. MT

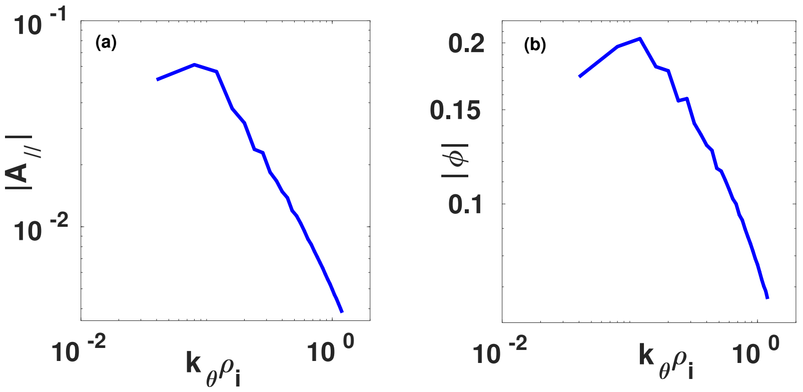
(a)
$|A_{//}|$
10^{-1}
10^{-2}
10^{-2}
10^{0}
$k_\theta\rho_i$
(b)
$|\phi|$
0.2
0.15
0.1
10^{-2}
10^{0}
$k_\theta\rho_i$

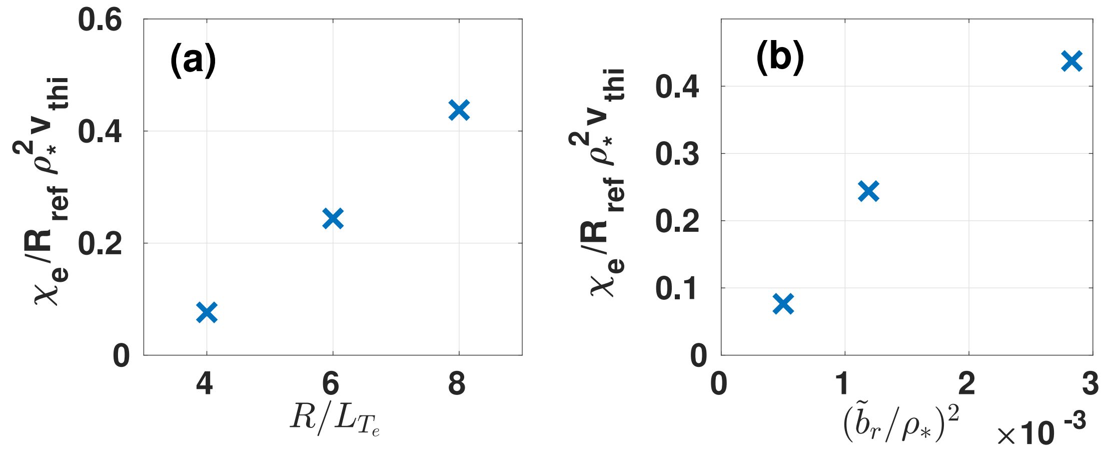
(a)
$\chi_e/R_{ref}\,\rho_*^2 v_{thi}$
0
0.2
0.4
0.6
4
6
8
R/L_{T_e}
(b)
$\chi_e/R_{ref}\,\rho_*^2 v_{thi}$
0
0.1
0.2
0.3
0.4
0
1
2
3
$(\tilde{b}_r/\rho_*)^2$
$\times 10^{-3}$

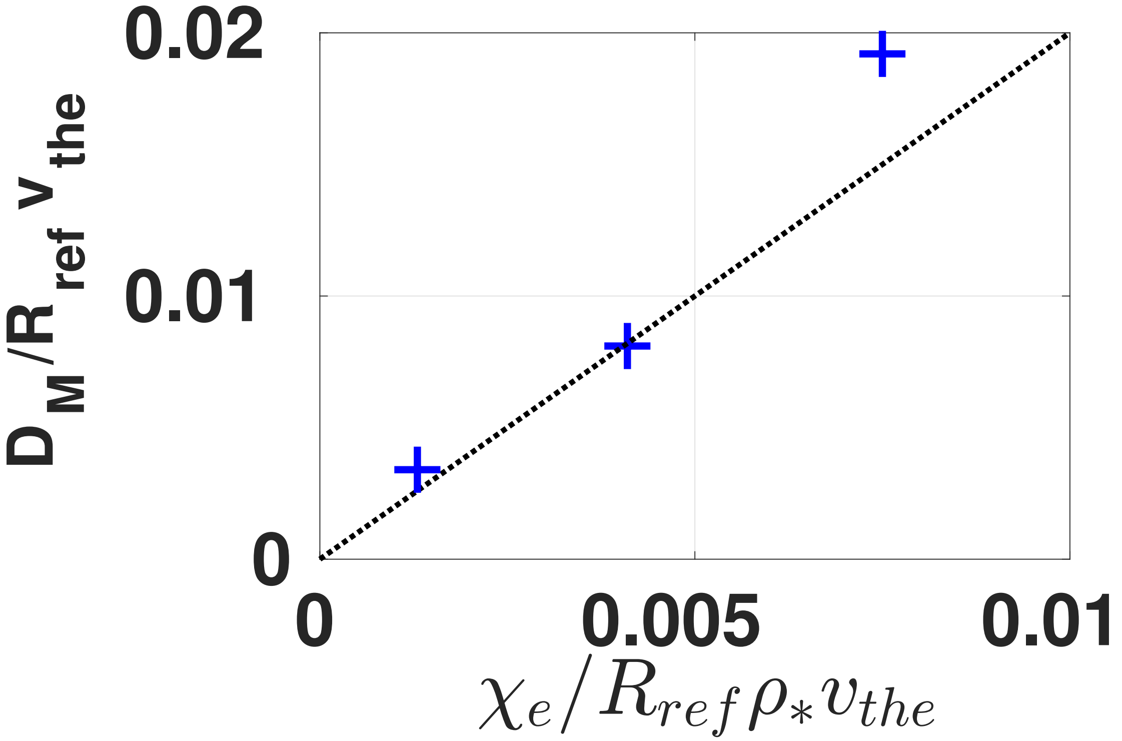
$D_M/R_{ref}\ v_{the}$
0.02
0.01
0
0
0.005
0.01
$\chi_e/R_{ref}\rho_* v_{the}$

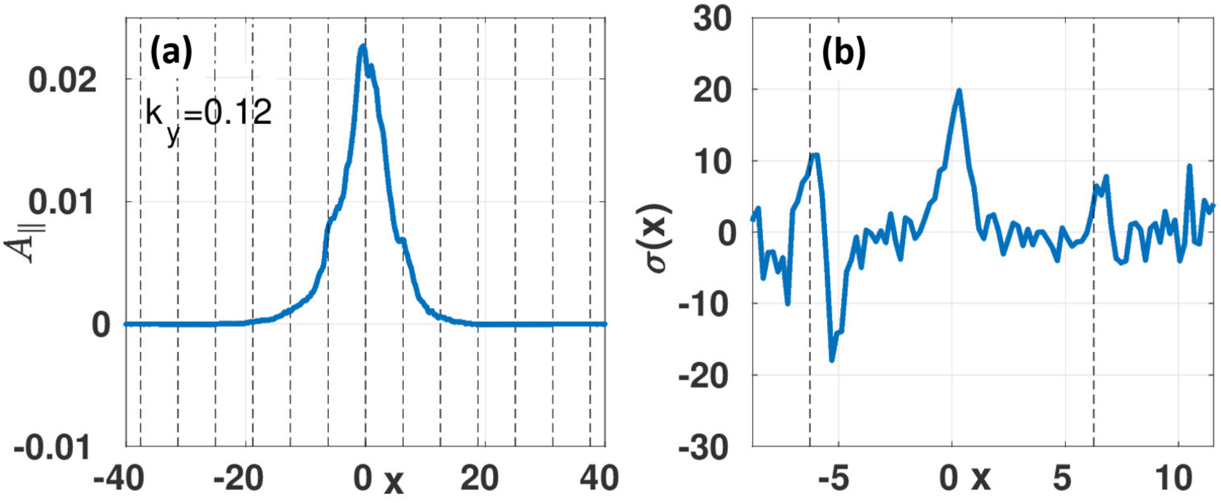
(a)
k_y=0.12
$A_\|$
0.02
0.01
0
-0.01
-40
-20
0
x
20
40
(b)
σ(x)
30
20
10
0
-10
-20
-30
-5
0
x
5
10

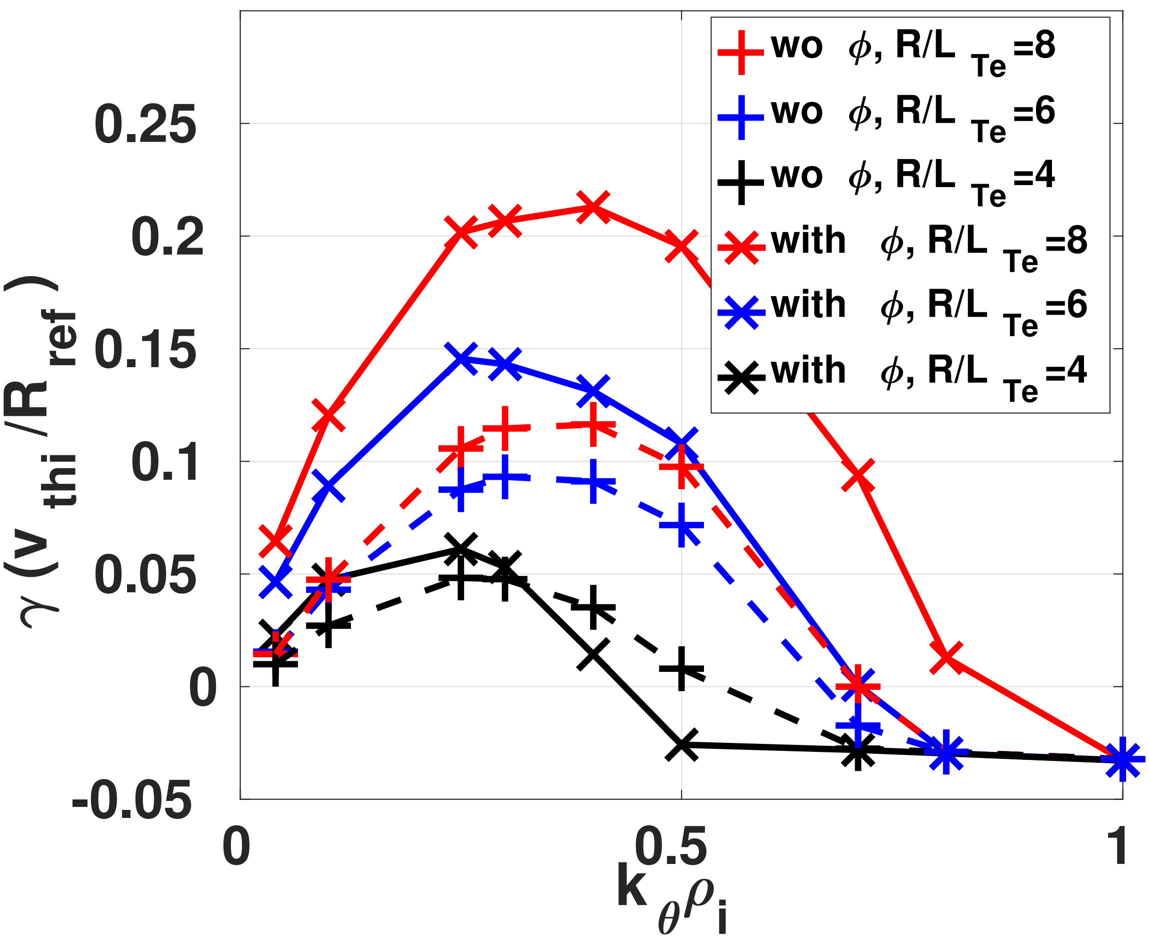
wo ϕ, R/L $_{Te}$=8
wo ϕ, R/L $_{Te}$=6
wo ϕ, R/L $_{Te}$=4
with ϕ, R/L $_{Te}$=8
with ϕ, R/L $_{Te}$=6
with ϕ, R/L $_{Te}$=4
γ (v$_{thi}$ /R$_{ref}$)
0.25
0.2
0.15
0.1
0.05
0
-0.05
0
0.5
1
k$_\theta \rho_i$

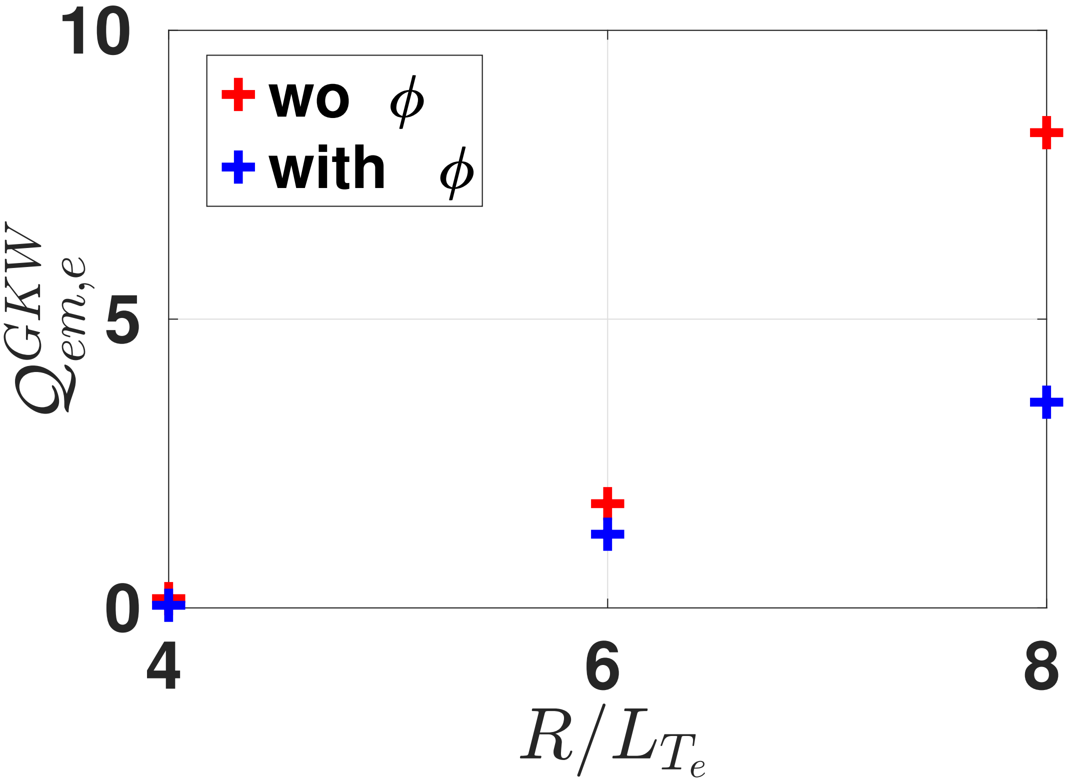

🟥 wo ϕ
🟦 with ϕ
$Q_{em,e}^{GKW}$
10
5
0
4
6
8
R/L_{T_e}

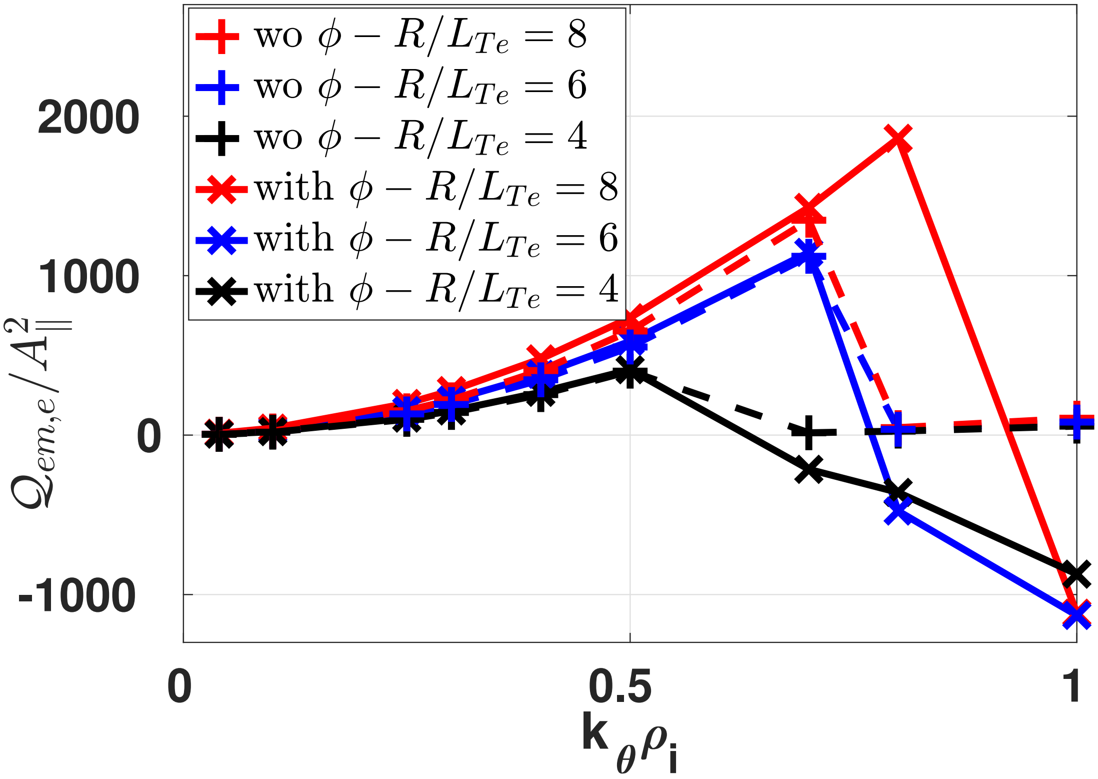
wo $\phi - R/L_{Te} = 8$
wo $\phi - R/L_{Te} = 6$
wo $\phi - R/L_{Te} = 4$
with $\phi - R/L_{Te} = 8$
with $\phi - R/L_{Te} = 6$
with $\phi - R/L_{Te} = 4$
2000
1000
0
-1000
$Q_{em,e}/A_{\|}^2$
0
0.5
1
$k_\theta \rho_i$

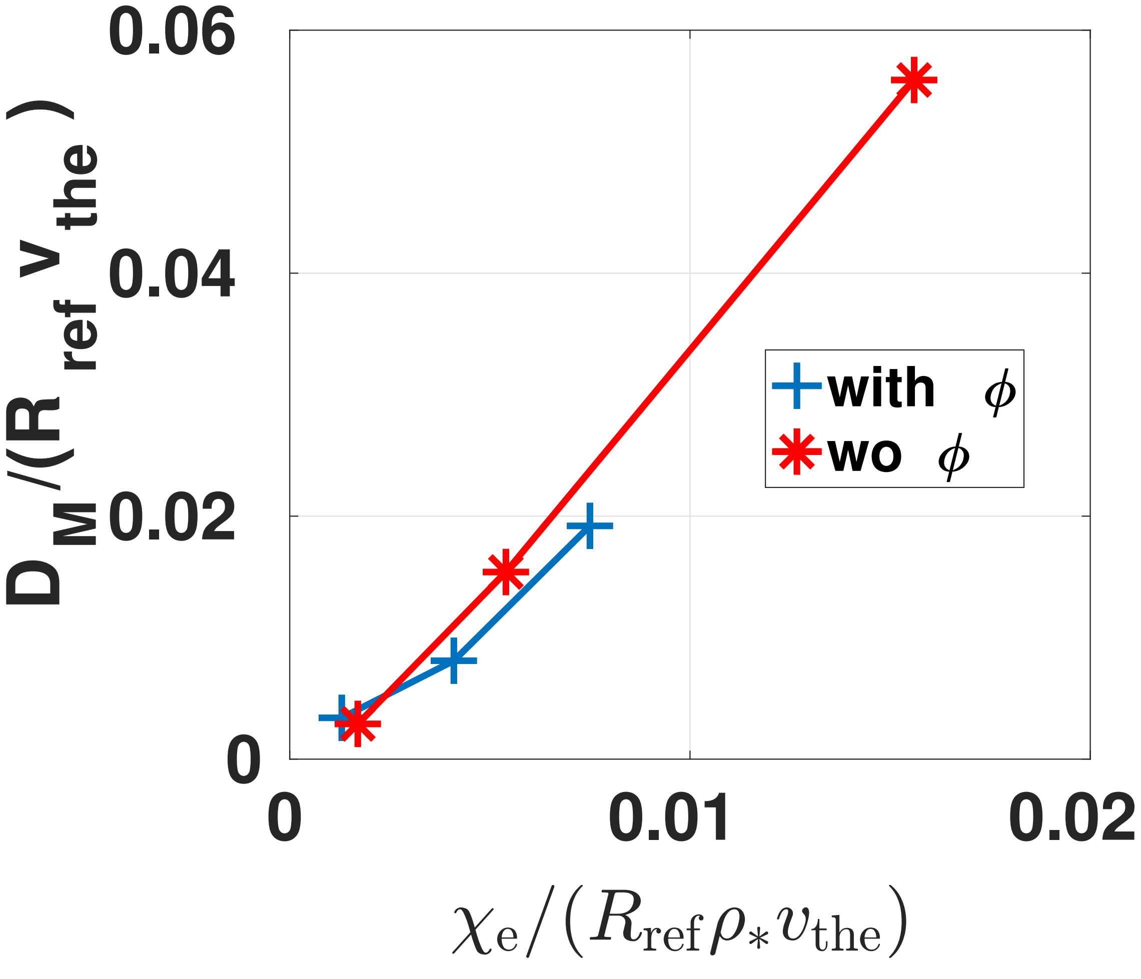
0.06
0.04
0.02
0
$D_M/(R_{ref}\, v_{the})$
0
0.01
0.02
$\chi_e/(R_{ref}\rho_* v_{the})$
with ϕ
wo ϕ

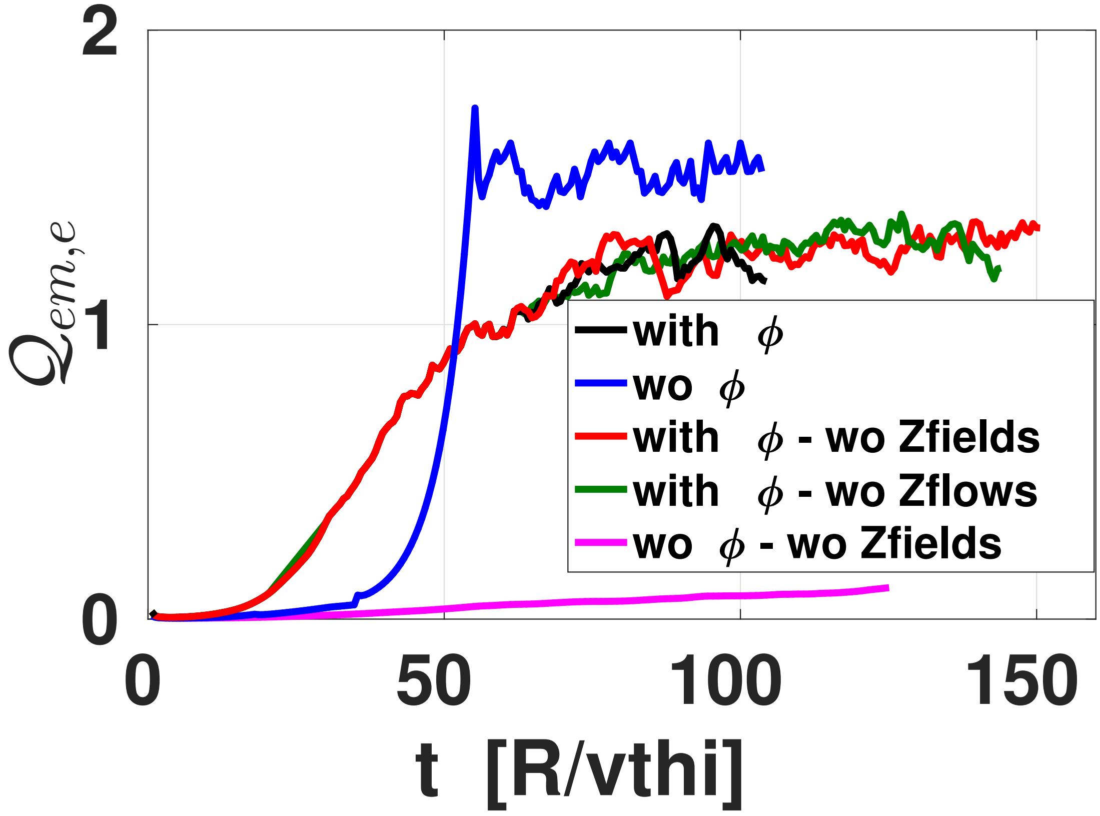
2
1
0
$Q_{em,e}$
0
50
100
150
t [R/vthi]
with ϕ
wo ϕ
with ϕ - wo Zfields
with ϕ - wo Zflows
wo ϕ - wo Zfields

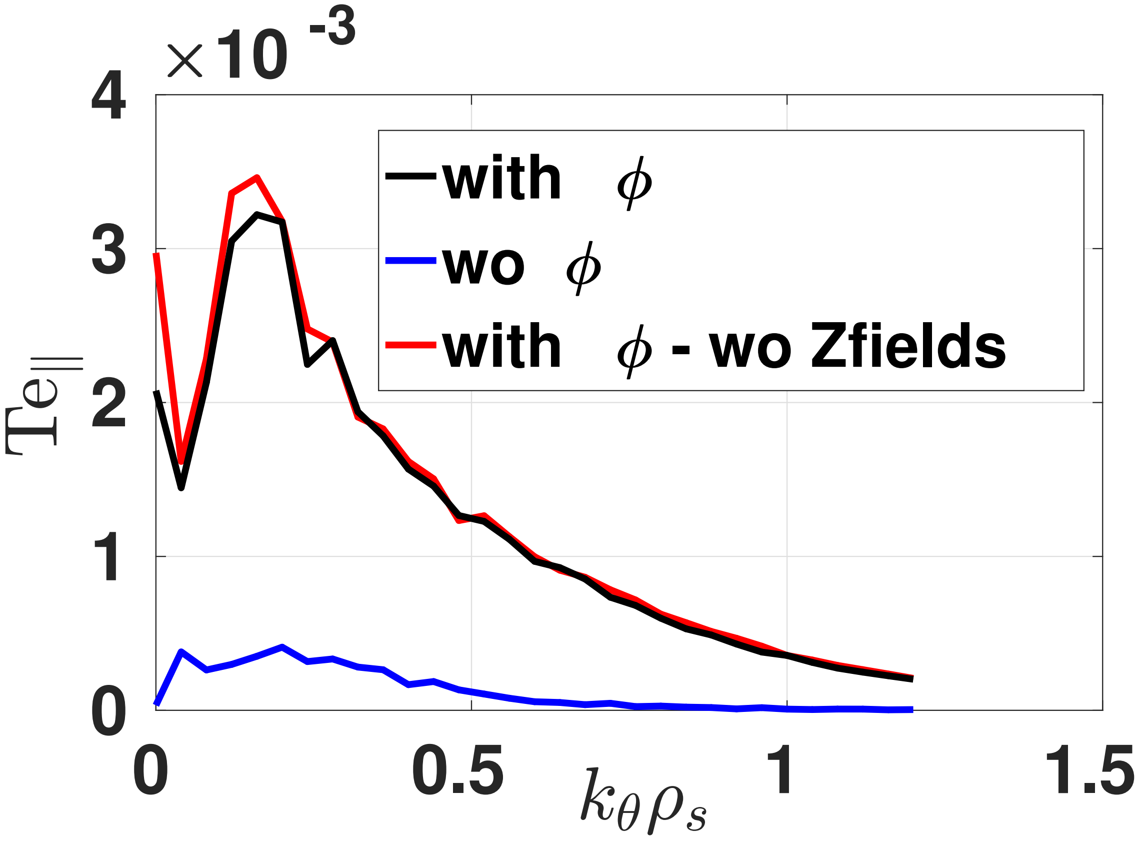
$\times 10^{-3}$
4
3
2
1
0
$Te_{||}$
0
0.5
1
1.5
$k_\theta \rho_s$
with ϕ
wo ϕ
with ϕ - wo Zfields